

Modelling of optimized shear scenarios with LHCD for high performance experiments on JET

T.J.J. Tala^a, F.X. Söldner^b, V.V. Parail, Yu.F. Baranov, A. Taroni^b
JET Joint Undertaking, Abingdon, Oxfordshire, United Kingdom

J.A. Heikkinen, S.J. Karttunen
Association Euratom–Tekes, VTT Chemical Technology, Espoo, Finland

Abstract. Modelling of LHCD with transport calculations is performed with the JETTO transport code, which has been upgraded by implementing the Fast Ray Tracing Code to calculate self-consistent LH power deposition profiles. Heat and particle transport models that are able to reproduce the experimental JET temperature and density profiles are used in JETTO for predictive high performance modelling. Application of 3.5 MW LHCD power provides an inverted q profile across 50–70% of the plasma radius whereas, without LHCD, the q profile is monotonic during the flat-top phase. The results predict that the fusion power is about 60% higher for high performance DT plasmas in the optimized shear scenario with 3.5 MW LHCD applied during the high performance phase than without LHCD at $B_t = 3.4$ T and $I_p = 3.9$ MA on JET. In addition, the width of the internal transport barrier (ITB) is 0.25–0.30 m larger and the ITB can be sustained for a longer time with LHCD.

1. Introduction

Advanced steady state tokamak operation with pressure and current profile control has become now one of the main goals of magnetic confinement fusion research. Rapid progress in performance has been made in recent experiments with this approach. Internal transport barriers (ITBs) have improved core energy confinement. Improvement of MHD stability with reversed central magnetic shear also gives access to higher β values, resulting in large bootstrap currents. Thus, moderate external current drive should be sufficient to supplement the bootstrap currents for steady state operation. The key to sustained high performance in the advanced steady state tokamak operation mode is a continuous control of pressure and current profiles.

Improved core confinement in a tokamak plasma is achieved by current profile modifications in high performance experiments [1]. The current profile can be modified with early heating by ICRH or LHCD during the current rampup phase. The modified current profile together with a steep pressure gradient gives rise to reduced transport which manifests itself as a further peaking of the temperature and density

profiles with steep gradients typically at $r/a = 0.5$ – 0.7 . These ITBs have a large influence on plasma core confinement and thereby significantly enhance tokamak performance [2–4]. This operation mode in JET where one of the key elements is the ITB is called the optimized shear (OS) scenario. At present it is considered to be the most promising approach towards steady state tokamak operation.

The operation mode with ITBs characteristic of the OS regime combined with an edge transport barrier of the high confinement H mode regime is called the double barrier (DB) mode. It has resulted in a fusion gain Q higher by a factor of 2 than those in conventional sawtoothed steady state ELMy H mode plasmas [5]. In DT discharges the DB mode has produced a fusion gain of $Q = 0.4$, and high performance has been sustained for four energy confinement times in the DB mode in a DD plasma. Recently, the DB mode has been routinely established in the gas box divertor configuration on JET.

Advanced tokamak scenario modelling with an optimized magnetic shear configuration that exhibits an ITB was performed by transport simulations recently in Ref. [6]. The authors of that article explored the capability of off-axis electron cyclotron current drive to control the hollow current profile in the OS operation mode. The evolution of the thermal and the particle ITBs with a monotonic or slightly reversed q profile and large $\mathbf{E} \times \mathbf{B}$ rotation shear

^a *Permanent address:* Association Euratom–Tekes, VTT Chemical Technology, Espoo, Finland.

^b *Present address:* European Commission, Brussels, Belgium.

produced mainly by NBI and ICRH was studied in Ref. [7].

In this work, the performance perspectives of the profile controlled OS scenario are investigated and optimized with the JETTO transport code modelling calculations, using LHCD for current profile control. With LHCD, hollow current density profiles and a wider reduced magnetic shear region can be achieved [1]. Thus LHCD can provide wider ITB during the high performance phase. However, high performance OS experiments with LHCD have not been performed on JET. It is therefore important to investigate how LHCD affects the formation and sustainability of the ITB. With a direct influence on the magnetic shear and an indirect one through the electron heating, LHCD can influence the transport coefficients. The LH power deposition depends sensitively on the temperature and density profiles. Accordingly, self-consistent calculation of transport and LH ray tracing including wave absorption is required.

The JETTO transport code [8] has been upgraded by adding the Fast Ray Tracing Code (FRTC) [9], which is run inside JETTO. Lower hybrid current density and power deposition profiles can be modelled by using either the coupled JETTO/FRTC code, the stand-alone Baranov's ray tracing code (noted in this article as BRTC) [10] or experimental profiles of JET discharges. The self-consistent LH power deposition profiles produced by the JETTO/FRTC code can be thus compared with stand-alone ray tracing results or with the experimental results. In the following simulations, self-consistent current profile control with long pulse LHCD during the high performance phase calculated by JETTO/FRTC is applied, producing a significant amount of off-axis current.

The JETTO transport model is based on an empirical transport model which has been developed on JET and validated against several JET discharges [11–13]. The heat and particle transport models are further tested for OS discharges with L and ELMy H mode plasma edge, with the main emphasis on the formation and the expansion of the ITB. The transport model in Ref. [7] differs in some details from the model used in our transport calculations. In the study reported in Ref. [7], the reproduction of the JET OS pulses Nos 40542 and 40847 was found to be as good as the reproduction of those two pulses with our transport model.

The article is structured in the following way. Section 2 gives a brief characterization and

summary of the experiments in the OS regime on JET. The transport model used in the transport calculations is described and tested in Section 3. The current profile control with LHCD is the topic of Section 4. The LH power deposition profiles calculated by the coupled JETTO/FRTC code are presented and compared with the profiles calculated by the stand-alone ray tracing code. The improvements in the ITB formation with LHCD for OS plasmas are also discussed. The high performance steady state discharges, including the analysis of different current rampup schemes, in the OS scenario regime with JETTO modelling calculations are demonstrated in Section 5. The main plasma profiles and the parameters predicted by the modelling calculations with LHCD applied during the high performance phase are given and the MHD stability analysis is illustrated. Finally, the summary and the conclusions follow in Section 6.

2. Optimized shear experiments

The OS discharge pulse No. 40847 has achieved the second highest neutron production rate in JET deuterium discharges staying only 5% below the record, also obtained with an OS pulse. Pulse No. 40847 represents the standard scenario of the high performance OS discharge on JET, including the typical sequence of the different confinement regimes. The characteristic time evolution of the main plasma parameters for this pulse is shown in Fig. 1.

The discharge is initiated with a fast plasma current rampup and an early X point formation at $t = 0.8$ s. A short application of LHCD during the early current rampup phase $t = 0.4$ – 1.2 s assists in forming the required target q profile. ICRH is used for pre-heating from $t = 3$ s to $t = 5$ s to slow down the current inward diffusion. High power heating with NBI and ICRH rises up to a maximum from $t = 5.0$ s to $t = 5.4$ s. An ITB is formed in this pulse at $t = 5.3$ s. The peripheral plasma remains in L mode until $t = 6.76$ s when a transition to an ELM-free H mode occurs. The ion heat conductivity falls close to the neoclassical level in the plasma core. The region of reduced heat conductivity expands gradually with the expansion of the ITB during the L mode phase. The ion heat conductivity is further reduced also in the peripheral region during the ELM-free H mode phase. MHD stability is maintained near the marginal stability limit with a real time power

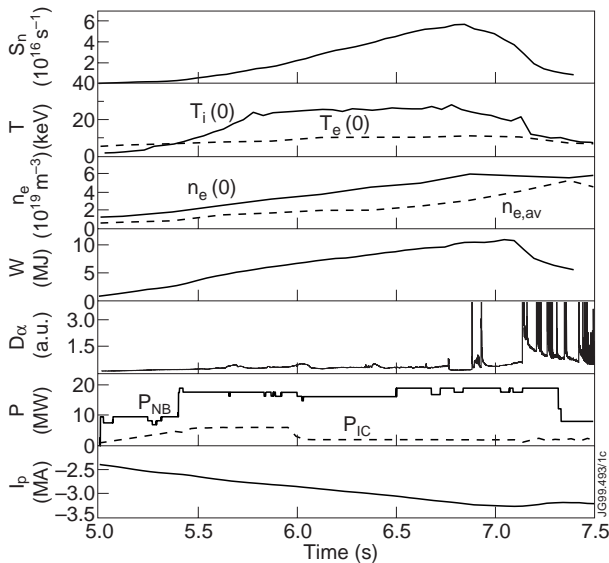


Figure 1. Time traces of the neutron rate S_n , the central ion T_i and electron T_e temperatures, the electron density n_e , the diamagnetic energy W , D_α signal, the heating powers P_{NB} and P_{IC} and the plasma current I_p for the OS discharge (pulse No. 40847) with an ITB and a long lasting L mode edge. The ITB appears at $t = 5.3$ s and the plasma edge experiences an L–H transition at $t = 6.76$ s.

control. At $t = 6.88$ s a first ELM marks the transition to an ELMy H mode phase. During this last phase the performance decreases and the ITB decays.

JET pulse No. 40542 represents a discharge in the DB mode. Internal and external transport barriers are superposed in the OS scenario with the plasma edge in ELMy H mode. The discharge approaches steady state conditions in its temperature and density profiles. High performance with an H factor $H^{89-P} \approx 2$ has been maintained for four energy confinement times. An ITB is formed in this pulse at $t = 5.4$ s. The peripheral plasma remains in L mode until $t = 6.2$ s when a transition to an ELMy H mode occurs. The H mode adds an edge transport barrier (ETB) to the persisting ITB. Both transport barriers co-exist for the remaining phase of high power heating until the NBI power is ramped down from $t = 7.5$ s onwards. Only this ends the high performance steady state phase. The time traces for this pulse are illustrated in Fig. 2.

The ion heat conductivity χ_i falls to the neo-classical level in the plasma core. The region of reduced heat conductivity expands gradually out to two thirds of the plasma minor radius during the L mode phase. The extent of the improved core is

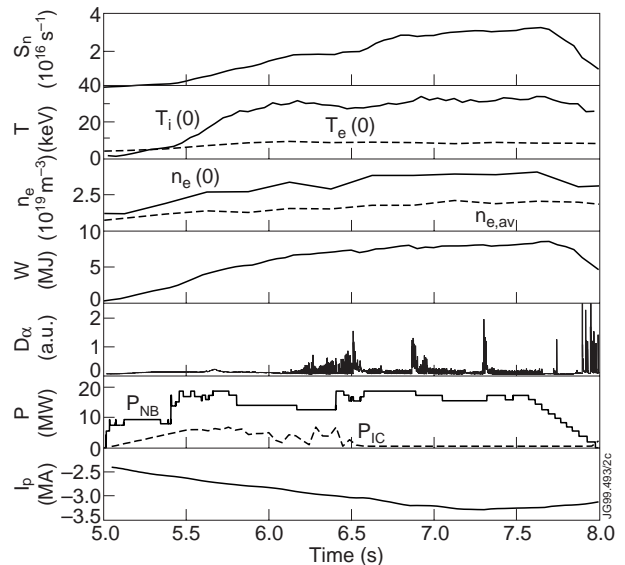


Figure 2. As in Fig. 1, but for the OS discharge (pulse No. 40542) with an ITB and ELMy H mode edge. The ITB appears at $t = 5.4$ s and the plasma edge experiences an L–H transition at $t = 6.1$ s. The DB mode exists until $t = 7.5$ s when the heating is turned down.

maintained during the H mode phase. The ion heat conductivity is further reduced by a factor of 3 in the peripheral region during ELMy H mode.

The electron heat conductivity χ_e is also reduced over the whole plasma cross-section and shows an ITB at the same location, as seen from the ion heat conductivity profile. The reduction in electron heat conductivity, however, is much smaller than that in ion heat conductivity. Inside the ITB, χ_e drops typically by a factor of 5, while χ_i falls by more than an order of magnitude.

MHD stability calculations show a gradual rise of the beta limit after the pressure profile broadening with the transition to ELMy H mode. The marginal stability limit for pressure driven kink modes then increases up to $\beta_N \approx 3$.

3. Description of the JETTO transport model

In this work, we will use as the basic model an empirical transport model developed at JET and tested against several different plasma discharges on DIII-D, TFTR, JT-60, ASDEX Upgrade, START and JET in L mode and against many different plasma discharges on JET in H mode [11, 12]. It is

based on a combination of a Bohm and a gyro-Bohm type of anomalous transport, and the set of transport coefficients can be written in the following form:

$$\chi_e = 1.0\chi_{gB_e} + 2.0\chi_B \quad (1)$$

$$\chi_i = 0.2\chi_{gB_i} + 4.0\chi_B + \chi_i^{neo} \quad (2)$$

$$D = [w_1 + (w_2 - w_1)\rho_{eff}] \frac{\chi_e\chi_i}{\chi_e + \chi_i} \quad (3)$$

where

$$\chi_{gB_{e,i}} = 5 \times 10^{-6} \sqrt{T_{e,i}} \left| \frac{\nabla T_{e,i}}{B_t^2} \right| \quad (4)$$

$$\chi_B = 4 \times 10^{-5} R \left| \frac{\nabla n_e T_e}{n_e B_t} \right| q^2 \times \left(\frac{T_e(0.8\rho_{max}) - T_e(\rho_{max})}{T_e(\rho_{max})} \right). \quad (5)$$

In Eqs (4) and (5), T_e and T_i are the electron and the ion temperatures, respectively, n_e is the electron density, B_t the toroidal magnetic field, R the major radius and q the safety factor. χ_i^{neo} is the neo-classical term for the ion heat transport. The non-locality in the Bohm transport appears in the last term where ρ_{eff} is the flux surface label defined by $\rho_{eff} = \sqrt{\Phi/\pi B_t}/a_{eff}$ with a_{eff} being the radius of the circle covering the same area as the elongated plasma. ρ_{max} is the value of ρ_{eff} at the separatrix in L mode and on top of the barrier in H mode and Φ is the toroidal magnetic flux. All the quantities appearing in Eqs (1)–(8) are expressed in SI units except the temperatures T_e and T_i whose units are electronvolts. w_1 and w_2 , which are multipliers to the particle diffusion coefficient, are the only coefficients that are varied in the model in Eqs (1)–(5). The boundary temperatures for the ions and electrons are taken from the experiment. Modelling of the boundary particle transport is not a well understood problem and we have solved it by assuming that the recycling coefficient at the separatrix is equal to one and then using the experimental particle flux through the separatrix to determine the particle losses from the plasma. The initial q profile is calculated by EFIT and Z_{eff} is taken from the TRANSP analysis.

The model for triggering the ITB is introduced with a step function switching off the Bohm transport when a control parameter exceeds a certain value [13]. The suppression condition of this dimensionless control parameter and the modified Bohm transport can be thus written as

$$s - \alpha_{e,i}\Omega < 0 \quad (6)$$

where

$$\Omega = \frac{\omega_{E \times B}}{\gamma} \propto \frac{R \left| \frac{(RB_\theta)^2}{B} \frac{\partial}{\partial \Psi} \left(\frac{\nabla n_i T_i}{en_i RB_\theta} \right) \right|}{v_{thi}} \quad (7)$$

$$\chi_{B_{e,i}} = \chi_B \Theta(s - \alpha_{e,i}\Omega) \quad (8)$$

where s is the magnetic shear, Ω the ratio of shear in poloidal plasma rotation to instability growth rate, Ψ the poloidal magnetic flux, B_θ the poloidal magnetic field, e the electron charge and $\gamma = v_{thi}/R$ the characteristic growth rate of the drift type of plasma turbulence, with α_e and α_i being the numerical weighting factors for shear in plasma rotation Ω for electrons and ions, respectively. The Θ function multiplying the modified Bohm transport in Eq. (8) is the normal Heaviside step function with the controlling parameter given by Eq. (6). The physical meaning of the step function is that in regions where the argument $s - \alpha_{e,i}\Omega < 0$, the Bohm type of anomalous transport is fully suppressed, i.e. $\Theta = 0$, which then leads to the formation of the ITB. The contributions from the toroidal and poloidal velocities to the radial electric field and Ω are omitted in this model because of the difficulties in modelling the toroidal velocity and due to the lack of measurements of the poloidal rotation on JET [14]. A model which takes into account all three terms in the radial electric field is under construction for the JETTO transport code and the preliminary results are published in Ref. [15]. In consequence, there are four numerical parameters to be fitted with the experimental data, the coefficients α_e and α_i for triggering the ITB as well as the earlier defined w_1 and w_2 in the particle transport.

The model has been tested in the OS regime against both the ITB formation in L mode and ITB formation with ELMy H mode discharges on JET. In Fig. 3, we have reproduced one steady state ITB pulse with first L mode edge till $t = 6.2$ s and then later with ELMy H mode edge (pulse No. 40542, which was already illustrated in Section 2, Fig. 2). In particular the heat transport model can describe the temporal evolution of $T_{e,av}$ and $T_{i,av}$ mostly within the experimental error bars, but despite some further development of the particle transport model moderate uncertainties still persist in it. The differences in the time traces at around $t \approx 6.2$ s are related to the difficulties that the model has in following the rapid L–H transition at the plasma edge. After the delayed response to the L–H transition the transport model reproduces the experiment again nearly within the error bars after $t = 6.5$ s. In this analysis, the values $\alpha_e = 0.0$ and $\alpha_i = 1.9$ were chosen for electrons

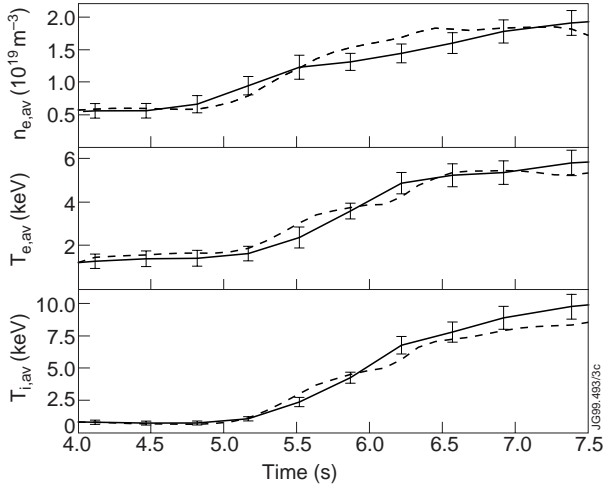


Figure 3. Reproduction of JET deuterium discharge No. 40542. The solid curves with error bars correspond to the experiment and the dashed curves are given by our transport model. The time evolution of the volume averaged electron density and the average electron and ion temperatures are shown.

and ions, respectively, as well as $w_1 = 0.8$ (core) and $w_2 = 0.3$ (edge) for the multipliers to the particle transport.

To quantify the agreement between the modelling and the experiments, a statistical approach to simulation results is applied according to the equations

$$m_Y = \left(\sum_{i=1}^K \frac{\sum_{j=1}^N (Y_{exp}(x_j) - Y(x_j))/Y(x_j)}{N} \right) / K \quad (9)$$

$$\Delta_Y^2 = \sum_{i=1}^K Z_i / K \quad (10)$$

where Z_i is defined as

$$Z_i = \frac{\sum_{j=1}^N (Y_{exp}(x_j) - Y(x_j) - m_{Y,i})/Y(x_j)^2}{N}. \quad (11)$$

The calculated quantity m_Y symbolizes the modelling offset of the quantity Y , which can be in our case either n_e , T_e or T_i , and the quantity Δ_Y^2 stands for the variance between the experimental measurement and the modelling result of the quantity Y . The inner summation from 1 to N is over the radial grid points ($N = 51$) and the outer summation is over 15 ($K = 15$) time points evenly distributed within the time interval of the simulation. $m_{Y,i}$ is the value

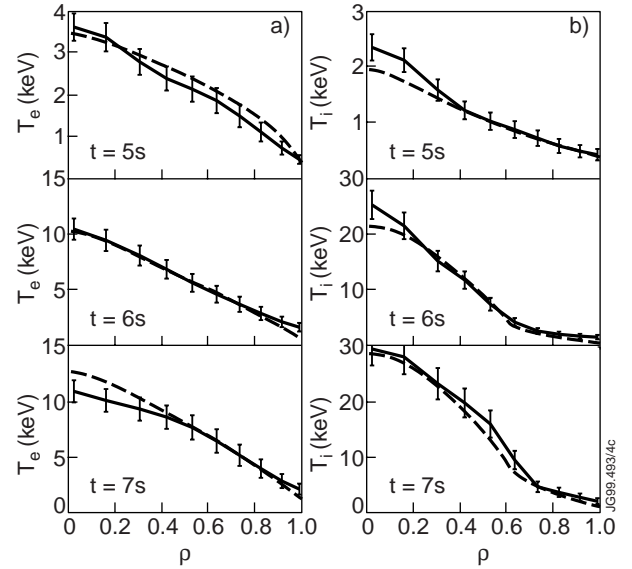


Figure 4. Radial profiles of (a) the electron and (b) the ion temperatures for the reproduction of JET deuterium discharge No. 40542. The solid curves correspond to the experiment and the dashed curves are given by our transport model.

of m_Y without the sum over the time range K at the i th time step. $Y_{exp}(x_j)$ is the measured value of the given quantity at the radial point x_j and $Y(x_j)$ is the calculated value at the same point. Consequently, m_Y and Δ_Y^2 characterize the time average modelling offset and the time average modelling variance compared with the measurement over the whole duration of the simulation.

The radial profiles of the electron and ion temperatures as a function of $\rho = r/a$ at $t = 5.0$ s, $t = 6.0$ s and $t = 7.0$ s are presented in Figs 4(a) and (b), respectively. The central ion temperature is underestimated at $t = 5.0$ s and $t = 6.0$ s, but otherwise the profiles are in good agreement with the experiment, mostly within the error bars. In Fig. 5, the density and pressure profiles are shown at the same three instants. The modelling results are well within the error bars in H mode, but in L mode the model tends to overestimate the density. The calculated modelling offsets and modelling standard deviations for T_e , T_i and n_e are presented in Table 1. The standard deviations for the heat transport Δ_{te} and Δ_{ti} , calculated over the whole simulation period (from $t = 4.0$ s up to $t = 7.5$ s), are clearly smaller than the standard deviation of n_e when using the model with $\alpha_i = 1.9$ and $\alpha_e = 0$. Positive modelling offsets in Table 1 indicate that those quantities are

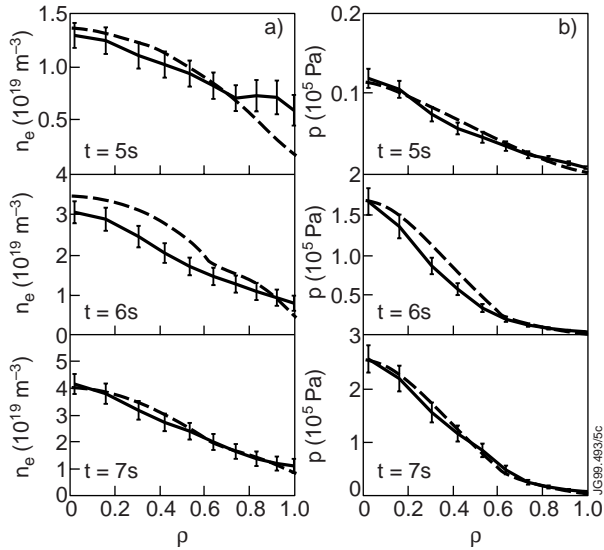


Figure 5. As in Fig. 4, but for (a) density and (b) pressure.

underestimated on average over the whole time range by the transport calculation.

The power deposition profiles of NBI and ICRH are calculated by TRANSP and shown in Fig. 6 at $t = 5.0$ s, $t = 6.0$ s and $t = 7.0$ s. The maximum power for NB heating is about 18 MW and for ICRH about 7 MW. The standard Monte Carlo model was used for calculating the NB power deposition profiles. For the calculation of the ICRH power deposition profiles, the bounce averaged Fokker–Planck code [16] was applied in TRANSP calculations. A comprehensive study of the use of that ICRH module inside TRANSP with OS plasmas and the analysis of ICRH for JET high performance plasmas is made in Refs [17, 18]. The frequency of the applied ion cyclotron hydrogen minority heating scheme (minority concentration 2–3%) was 51 MHz. The diamagnetic energy of the TRANSP analysis for this pulse is almost identical to the experimentally measured diamagnetic energy. Accordingly this can be regarded as an indirect proof of the goodness of the NBI and ICRH power deposition profiles because about 50% of W_{dia} comes from the contribution of the fast particles produced by NBI and ICRH.

The time evolution of the footpoint of the ITB is shown in Fig. 7. The dashed curve corresponds to the radius of the ITB observed in experiment (pulse No. 40542) and the solid curve is calculated by the transport model. The radial expansion of the ITB with time can be reproduced within 6 cm of the measured one by the model even if it tends to

Table 1. Modelling offsets m_{Te} , m_{Ti} and m_{ne} and the modelling standard deviations Δ_{Te} , Δ_{Ti} and Δ_{ne} for the best choice of α_i and α_e ($\alpha_i = 1.9$ and $\alpha_e = 0.0$) and the optimum case with $\alpha_i = \alpha_e$ for pulse No. 40542

α coefficients	m_{Te}	m_{Ti}	m_{ne}	Δ_{Te}	Δ_{Ti}	Δ_{ne}
$\alpha_i = 1.9, \alpha_e = 0.0$	-0.01	0.11	0.04	0.18	0.19	0.26
$\alpha_i = 1.2, \alpha_e = 1.2$	0.02	0.27	0.05	0.19	0.36	0.27

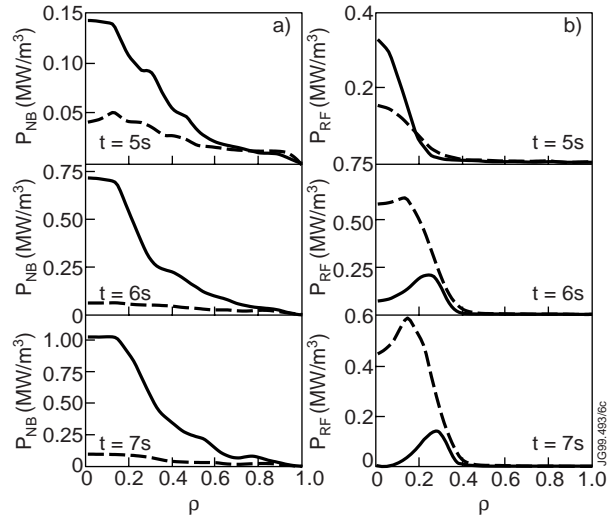


Figure 6. (a) NBI power deposition profiles and (b) ICRH power deposition profiles, both calculated by TRANSP at the same instants as the profiles in Figs 4 and 5. The solid curves correspond to the contribution to the ion heating and the dashed ones to the electron heating.

underestimate slightly the width of the barrier during the steady state phase.

The reason for fixing $\alpha_e = 0$ was that the shear in plasma rotation has only a weak or negligible effect on short wavelength turbulence which is mainly responsible for the electron heat transport. The reproduction is clearly better when $\alpha_e = 0$. The other motivated choice by the physics reasons for α_e would be $\alpha_i = \alpha_e$. In that case the optimum choice according to the modelling calculations is $\alpha_i = \alpha_e = 1.2$. However, the calculated standard deviations in Table 1 in the lower column, especially in Δ_{ti} , confirm the belief that $\alpha_e = 0.0$ was a justified choice.

The sensitivity analysis of the most critical numerical parameter α_i is shown in Fig. 8, where the width

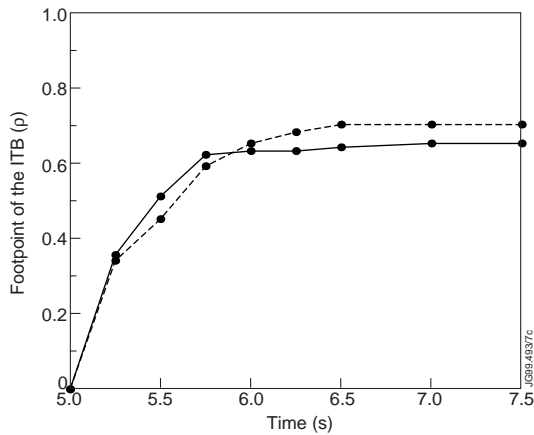


Figure 7. Radial location of the footpoint of the ITB as a function of time. The dashed curve is from pulse No. 40542 and the solid curve is calculated by the transport model.

of the ITB is plotted as a function of α_i at $t = 7.0$ s. As can be seen, the width of the ITB decreases almost linearly with decreasing α_i and the ITB vanishes when $\alpha_i < 0.8$. The same values $w_1 = 0.8$ and $w_2 = 0.3$ were applied during the previous sensitivity analysis. The model is only weakly sensitive to the values of w_1 and w_2 according to a comprehensive sensitivity analysis in the range of $w_1 = [0.2, 2.5]$ and $w_2 = [0.2, 2.5]$.

The most critical assumption in the model is that the initial q profile is taken from EFIT. As shown by Eq. (8), the magnetic shear s , or the q profile has a strong effect on the ITB formation and the width of the barrier. Consequently, the accuracy of the EFIT magnetic reconstruction plays a major role in the modelling calculations. However, by starting the simulation early enough, well before the main heating phase when the current has only about 50–70% of its flat-top value, the current evolution calculated by JETTO should have enough time to evolve in a self-consistent way independently of the initial q profile by EFIT. In all the previous analyses the simulations were started at least 1 s before the main heating phase. The optimum choice for α_i would be 10–20% higher (depending on the pulse) if the simulation was started at the same time as the main heating than in the case with the early start of the simulation. In the future, after validating the new motional Stark effect (MSE) magnetic measurements on JET, EFIT will produce more accurate q profiles.

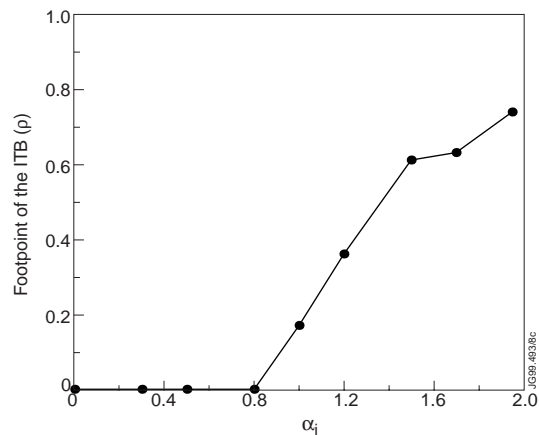


Figure 8. Radial location of the footpoint of the ITB as a function of the weighting factor α_i to shear in plasma rotation for pulse No. 40542 at $t = 7.0$ s.

4. Current profile control and improved ITB formation with LHCD

Lower hybrid current drive has been shown to be the most efficient of the various methods for non-inductive current drive in tokamaks so far and it has been used for current profile control in many experiments [19]. It can be applied in particular in off-axis current drive for creating or sustaining hollow current density profiles. Current profile control by LHCD has been explored and experimented with by using various techniques [2, 3, 20–22]. Another means to control the current profile evolution is current rampup, and its effect on optimizing the fusion performance is investigated in Section 5.1. In this section, we concentrate on the questions of modelling of LHCD current profile for high performance OS discharges and the results of modelling of the current profile control during the main heating and fuelling phase. Moreover, the improved ITB formation when applying LHCD during the main heating phase is considered.

4.1. Validation of self-consistently calculated LHCD by JETTO/FRTC

A new ray tracing code, called FRTC [9], has been installed and coupled to the JETTO transport code. The lower hybrid power deposition and current density profiles are calculated in a self-consistent way, i.e. the evolving temperature and density profiles as well

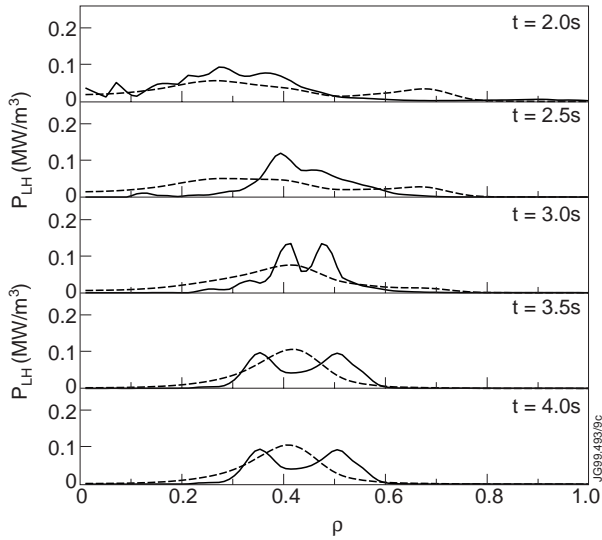


Figure 9. Lower hybrid power deposition profiles calculated by the coupled JETTO/FRTC code (solid curves) and BRTC (dashed curves) for pulse No. 47952.

as the poloidal magnetic field are read directly from JETTO by FRTC at each time step when FRTC is called. The calculated power deposition and current density profiles by FRTC are then used as the source terms for further time steps in JETTO, thus creating a self-consistent transport calculation with current profile control by LHCD. In FRTC, the flux surface averaged quasi-linear diffusion coefficient is found from the power deposition profiles and then used in a 1-D Fokker–Planck equation to calculate the electron distribution function. The equilibrium between the electron distribution and the power deposition is thus achieved by iteration, and finally the driven current can be evaluated. The 1-D Fokker–Planck equation is as in Ref. [23], except in FRTC the collision frequency has the factor $10/(5 + Z_{eff})$ instead of $2/(2 + Z_{eff})$. This accounts for the important corrections observed with the 2-D Fokker–Planck equations over 1-D solutions, i.e. enhancement of the current drive efficiency by a factor of 2.5 for $Z_{eff} = 1$ and the slight increase of this factor with Z_{eff} .

The power deposition profiles calculated by the coupled JETTO/FRTC code (solid curves) and the profiles that are calculated by BRTC [10] (dashed curves) are compared in Fig. 9 for pulse No. 47952. The maximum input heating powers for this recent LHCD profile control discharge are $P_{LH} = 1.4$ MW and $P_{NB} = 0.9$ MW, and the axial electron and ion temperatures vary between 2.0 and 3.5 keV as well as the axial electron density in the range $(1.1\text{--}1.7) \times 10^{19} \text{ m}^{-3}$. In each simulation, temperatures,

density and I_p were taken from the experiment throughout the pulse and the only transport equation that was solved was the current diffusion equation. Power deposition profiles given by JETTO/FRTC are in a reasonably good agreement with profiles from the stand-alone BRTC, as shown in Fig. 9. That argument can be also strongly motivated by following the time behaviour of the corresponding q profiles presented in Fig. 10. The q profile evolution is almost identical to the LH profiles found by JETTO/FRTC and by BRTC, whereas without LHCD, the q profiles are completely different, i.e. they are flat or monotonic rather than strongly reversed as with LHCD. Since the q profiles calculated by JETTO/FRTC and by BRTC are almost identical, the differences in the power deposition profiles, mostly due to stronger smoothing used in BRTC, do not affect significantly the evolution of the q profile. However, in general it cannot be concluded that the evolution of the q profile is not sensitive to LHCD (see the dotted curves in Fig. 10). Consequently, this can be regarded as an indication of the significant agreement between the LH calculation results of FRTC and BRTC, in spite of differences in the detailed structure in LH power deposition profiles. A more comprehensive study of the properties of FRTC and its power deposition profiles has been done in Ref. [24]. Due to the lack of LHCD experiments during the high performance phase on JET, the corresponding comparison of LH profiles calculated by the two codes under those circumstances could not be accomplished.

Measurement data from the fast electron bremsstrahlung (FEB) diagnostics are not available for pulse No. 47952, and thus the comparison with FRTC calculations could not be made. However, when comparing older LH discharges, pulses Nos 39274 and 39275, FRTC gives more localized power deposition profiles, and the peak of the deposition profile is located closer to the centre of the plasma than with the profiles from the Abel inverted FEB measurements. In addition, Abel inverted FEB profiles are much smoother. The difference between FRTC and Abel inverted FEB calculations can be due to the following three problems. Firstly, FEB diagnostics do not measure fast electrons with energies of less than 133 keV. Secondly, the other problem with FEB measurements is that they also count the X ray emission from the wall produced by the scattering and reflection processes. On the other hand, FRTC does not take into account the spatial diffusion the fast electrons.

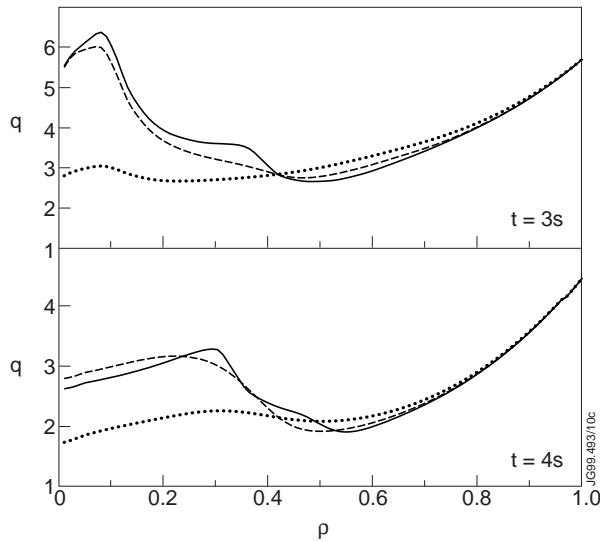


Figure 10. Evolution of the q profile calculated by the coupled JETTO/FRTC code (solid curve), by JETTO with LH power deposition profiles from the stand-alone BRTC (dashed curve) and without LHCD (dotted curves) for pulse No. 47952.

4.2. Improved ITB formation with LHCD

The negative or small magnetic shear s resulting from the hollow or flat current density profile is one of the two key factors suppressing the Bohm transport, as can be seen in Eq. (6). However, it has not been clear how large the effect of LHCD power and the deposition profiles on the formation and location of the internal transport barrier is due to the lack of experiments where LHCD has been applied during the high performance phase on JET. Consequently, this issue was analysed by using the JETTO transport code with self-consistent LHCD deposition profiles from FRTC.

Current profile control with off-axis LHCD has been applied during the high performance phase to freeze the q profile by heating the electrons, thus causing the current diffusion to slow down. Moreover, it provides additional off-axis current peaked at about $\rho = 0.6$ – 0.8 giving rise to a larger region of low magnetic shear. This dual effect of the current profile control can be seen in Fig. 11. The plasma parameters and initial temperature, density and q profiles are from pulse No. 40542. The input heating powers and power waveform of NBI and ICRH are as shown in Fig. 6 and after that the NBI and ICRH power deposition profiles are kept fixed until $t = 10.0$ s at the level of $P_{NB} = 18$ MW and $P_{RF} = 6.5$ MW. The

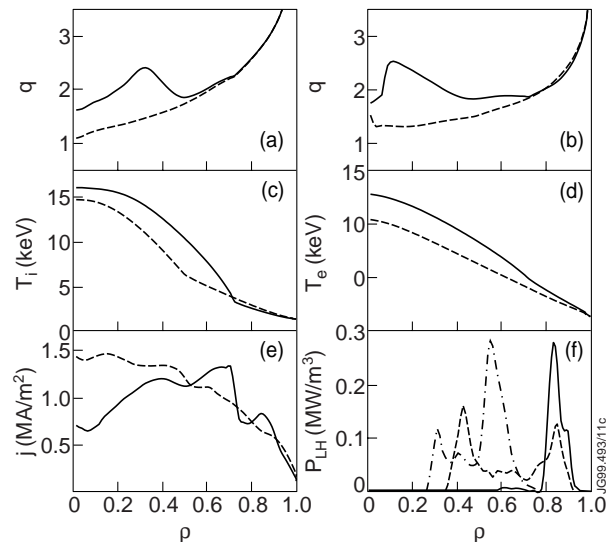


Figure 11. (a) Profiles of q with 3.5 MW LHCD (solid curves) and without LHCD (dashed curves) at $t = 6.0$ s and (b) at $t = 10.0$ s for the high performance OS modelling discharge. (c) The ion and (d) the electron temperature and (e) the current density profiles with (solid curves) and without (dashed curves) LHCD at $t = 10.0$ s. (f) The LH power deposition profiles from JETTO/FRTC at $t = 6.0$ s (chain curve), $t = 8.0$ s (dashed curve) and $t = 10.0$ s (solid curve).

values of the numerical variables were kept the same as those in Section 3, i.e. $\alpha_e = 0.0$ and $\alpha_i = 1.9$ as well as $w_1 = 0.8$ and $w_2 = 0.3$.

Application of 3.5 MW LH power with power deposition and current density profiles calculated self-consistently by JETTO/FRTC provides an inverted q profile across 50–70% of the plasma radius, whereas the q profile is monotonic without LHCD. The reversed region in the q profile becomes wider from the early main heating phase at $t = 6.0$ s until $t = 10.0$ s, and the changes at the plasma periphery are due to continuous current rampup up to $I_p = 3.9$ MA. Thus, LHCD provides off-axis current drive in these conditions and creates a broad hollow current profile as is seen in Fig. 11(e). Worth mentioning here is the great significance of the amount the bootstrap current, which is about 50% of the total current. The large contribution from the bootstrap current ($\gtrsim 50\%$) due to the large pressure gradient over a wide region of high density in the core plasma is typical of these high performance OS plasmas according to the modelling calculations.

The radial expansion of the ITB from $\rho \approx 0.5$ to $\rho \approx 0.7$ due to LHCD is seen in Fig. 11(c), where

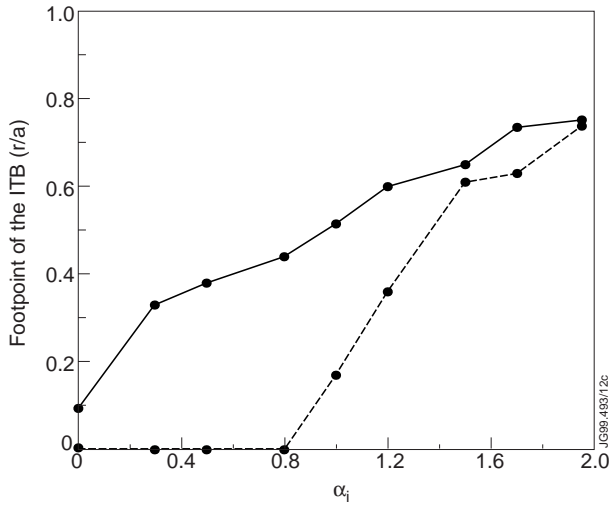


Figure 12. Radial location of the footpoint of the ITB as a function of the weighting factor α_i to shear in plasma rotation at $t = 7.0$ s. The solid curve corresponds to the case with 3.5 MW LHCD and the dashed curve without LHCD (pulse No. 40542).

we have plotted the ion temperature with and without LHCD at $t = 10.0$ s. The electron temperature is also higher with an additional 3.5 MW LHCD, as shown in Fig. 11(d). Thus current diffusion slows down and steady state conditions with a more robust ITB can be sustained for a longer time. The pressure is also higher and the region with high pressure is wider with LHCD. Both these features give rise to the better fusion performance. The pressure in our calculations is of the same order as in the record fusion discharge (DT, hot ion H mode) on JET [25]. The LH power deposition profiles calculated by JETTO/FRTC are shown in Fig. 11(f).

The sensitivity of the formation and location of the ITB to the critical value of $\Theta(s - \alpha_{e,i}\Omega)$ used in our model for turbulence suppression was tested for the same plasma discharge (pulse No. 40542) with the same set of simulation parameters with and without off-axis current profile control by LHCD. In the model, we fixed $\alpha_e = 0.0$ as justified in Section 3, but α_i was varied to find out the sensitivity of the ITB formation and location to the weighting coefficient of the plasma rotation. This is shown in Fig. 12 at $t = 7.0$ s.

For lower values of α_i the stabilizing effect of shear in plasma rotation on the Bohm type of transport diminishes and the transport barrier shrinks. This dependence is significantly weaker with LHCD current profile control due to the wider flat shear

region. LHCD therefore does not just provide wider ITBs, but also stiffens the location and reduces radial fluctuations of its location due to slight variations in the shear. A similar curve was also calculated for the case with LH power of 7.0 MW, but this curve does not differ significantly from the one with 3.5 MW power. The case with $\alpha_i = 0.0$ corresponds to the situation where the shear in plasma rotation does not contribute to the barrier formation at all. As is illustrated in Fig. 12, with the only contribution from the magnetic shear the transport barrier would in that case be non-existent without LHCD and very narrow (width ≈ 10 cm) with LHCD. However, the experimental pulse No. 40542, where no LHCD was applied, had an ITB as shown, for example, in Fig. 4. Consequently, the contribution from magnetic shear cannot yield the ITB alone, but the contribution from the shear in plasma rotation has to be taken into account and thus α_i must be greater than 0.

5. High performance OS scenarios

5.1. Effect of the current rampup scheme on the current density profile and ITB

Magnetic configurations which have potential for both achieving high improved confinement factor and high β_N are characterized by broad or hollow current density profiles [26]. There are several methods to create such a configuration. One of the most promising is lower hybrid off-axis current drive, which was presented in Section 4. Another way to generate such a configuration is current rampup.

Current rampup plays an important dual role because it helps to establish a hollow current profile or flat q profile in the inner half of the plasma volume, but it also helps to keep plasma from turning into an H mode too early, presumably by keeping the H mode threshold high through driving high edge currents. Avoiding an early L–H transition is a key factor in building up high core pressure with an ITB [5]. Furthermore, the highest fusion performance in DD plasmas on JET has been obtained when an H mode transition was delayed as long as possible [1, 25].

We have analysed in a predictive way four different current rampup schemes with the JETTO transport code. Either the total plasma current or the current rampup speed is varied, but the other plasma and simulation parameters (except the toroidal

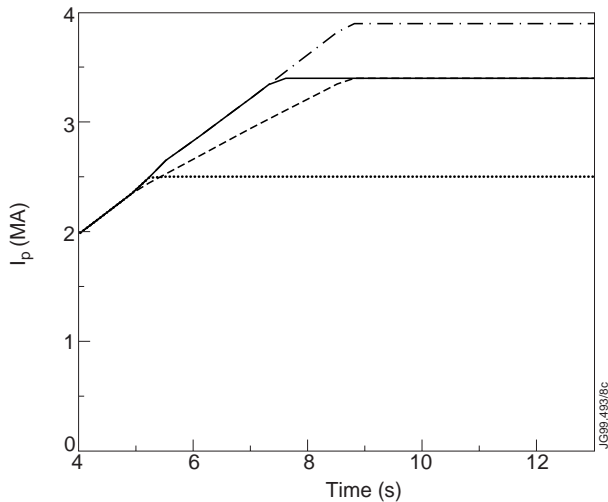


Figure 13. Four different current rampup schemes. The solid curve until $t = 7.5$ s corresponds to the experimental pulse No. 40542. The curves correspond to the following current rampup schemes: fast rampup speed ($dI_p/dt = 0.4$ MA/s) with flat-top value of $I_p = 3.9$ MA, chain curve; fast rampup with $I_p = 3.4$ MA, solid curve; slow rampup ($dI_p/dt = 0.28$ MA/s) with $I_p = 3.4$ MA, dashed curve; $I_p = 2.5$ MA, dotted curve.

magnetic field B_t that is varied in accordance with the steady state level of I_p) are kept fixed. The four different current rampup schemes used in this current rampup modelling of JET OS plasmas are presented in Fig. 13.

The current density, the magnetic shear s and the ion temperature profiles for these simulations are shown in Fig. 14 at $t = 10.0$ s when the plasma reaches the steady state level of the plasma current. The initial temperatures, density and q profile at $t = 4.0$ s were taken from pulse No. 40542. The current profiles are almost similar to each other in the core region. However, at radii larger than $\rho \approx 0.5$ they are strongly modified. The centre of the plasma is not affected due to the high electron temperature which effectively prevents current diffusion, whereas in the plasma periphery, the larger the plasma current, the more hollow is the current profile and correspondingly, the smaller is the magnetic shear. What is also interesting is that the faster current rampup (solid curve) with equal flat-top value of the current gives a more hollow current profile and thus smaller magnetic shear than the slower current rampup speed (dashed curve). This gives rise to higher temperature, larger pressure and thus larger fusion power.

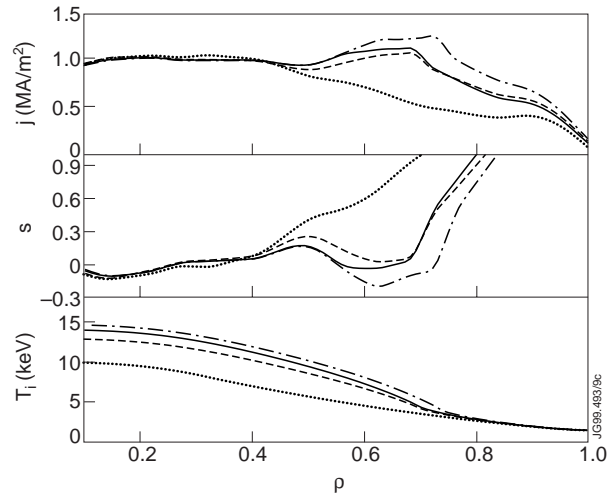


Figure 14. Current density j , magnetic shear s and ion temperature T_i profiles for the four current rampup schemes as presented in Fig. 13 with the same notations for the curves at $t = 10.0$ s.

The simple conclusion when comparing the different current rampup schemes is that with higher q_a (smaller I_p) shrinking of the ITB is caused by the higher edge shear. Accordingly, the region of low shear increases in size with lower q_a . This can be seen in Fig. 14 where the ITB in the ion temperature is at about $\rho = 0.35$ with $I_p = 2.5$ MA and at about $\rho = 0.73$ with $I_p = 3.9$ MA. Consequently, the best fusion performance for OS plasmas is expected to be obtained with the highest current and with the fastest stable current rampup speed, which was also confirmed on JET during DTE1 [27].

5.2. Fusion performance achieved with combined LHCD and fast current rampup

The starting point for the analysis of the high performance discharges with modelling calculations is the reproduction of pulse No. 40542, but the calculation is extended by 5 s beyond the real JET discharge. Consequently, the main heating phase lasts more than 5 s longer than the experiment and the plasma reaches steady state after $t = 10$ s. The reason for choosing this pulse initially and the main heating and fuelling phase until $t = 7.5$ s is that it has suitable steady-state-like features and benign properties against MHD instabilities. Due to the uncertainties persisting in the particle transport model, the multipliers w_1 and w_2 to the particle diffusion coefficient are varied and the differences in the

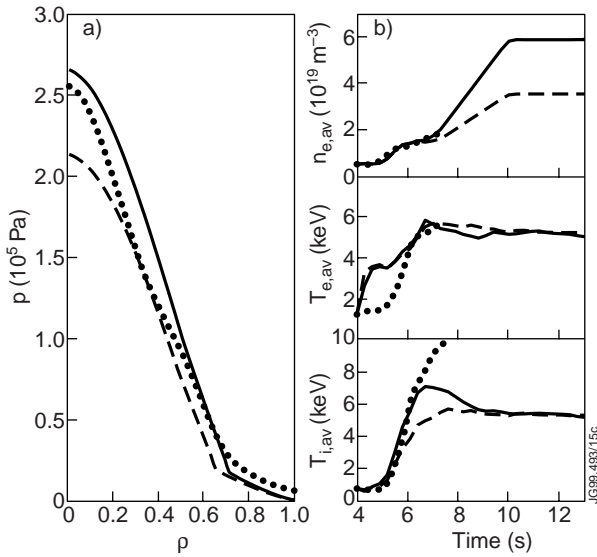


Figure 15. (a) Experimental pressure profile (dotted curve, pulse No. 40542) and two simulated pressure profiles with lower (solid curve) and higher (dashed curve) particle diffusion multipliers w_1 and w_2 at $t = 7.0$ s. (b) Average electron density and the average electron and ion temperatures with the same types of curve as a function of time.

performance predictions are illustrated. After a comprehensive sensitivity analysis of w_1 and w_2 in the range of $w_1 = [0.2, 2.5]$ and $w_2 = [0.2, 2.5]$ we show two different sets of w_1 and w_2 with the first set being $w_1 = 0.8$ and $w_2 = 0.3$ (set 1) and the second one $w_1 = 1.6$ and $w_2 = 0.6$ (set 2). Set 1 corresponds to the same values as used in Section 3 and set 2 represents a more conservative choice of w_1 and w_2 in the transport calculation. The plasma current is as for pulse No. 40542 until $t = 7.5$ s and afterwards it is as optimized in Section 5.1, i.e. the flat-top plasma current is 3.9 MA with fast current rampup speed and the toroidal magnetic field is 3.4 T. The heating power and the deposition profiles of NBI and ICRH have been kept fixed since the last experimental deposition profiles calculated by TRANSP. The NBI power deposition profiles did not change significantly according to PENCIL calculations although the density would be more than two times larger at $t = 10.0$ s. The LH power deposition profiles used in the analysis are calculated self-consistently by JETTO/FRTC.

The experimental pressure profile is better reproduced with the model with a lower particle diffusion multiplier (set 1) at $t = 7.0$ s, as shown in Fig. 15(a). The radial location of the ITB ($\rho \approx 0.7$) is well

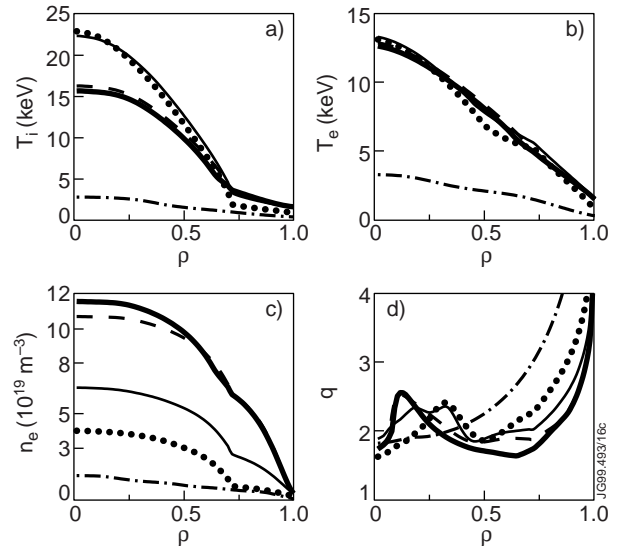


Figure 16. Radial profiles of (a) ion temperature, (b) electron temperature, (c) electron density and (d) q profile at: $t = 4.0$ s, chain curve; $t = 6.0$ s, dotted curve; $t = 8.0$ s, solid curve; $t = 10.0$ s, dashed curve; $t = 13.0$ s, thick solid curve.

reproduced by the model with smaller w_1 and w_2 whereas the model with larger w_1 and w_2 underestimates the width of the barrier. The pressure is slightly overestimated by the model with set 1 and strongly underestimated by the model with set 2. The time traces of the average electron density and the average electron and ion temperatures are illustrated in Fig. 15(b). The average density yielded by the model with set 1 is about 50% higher than in the model with set 2, partly due to smaller w_1 and w_2 , but mostly due to the smaller particle flux out of the plasma in the model with set 1. The differences in temperatures are much smaller between the models, but due to the applied LHCD power of 3.5 MW, the electron temperature in the simulated discharges is significantly higher especially at the beginning of the discharge. The experimental ion temperature is higher at $t \approx 7.5$ s, presumably for two different reasons. Firstly, because in the experiment NBI was turned down but ICRH was turned up again towards $t = 8$ s, whereas in the modelling calculations the powers of NBI and ICRH are on the same level as at $t = 6$ s and, secondly, due to the tendency for the model to underestimate slightly the ion temperature as shown already in Figs 3 and 4.

The evolution of the radial profiles is illustrated in Fig. 16. The ion temperature rises rapidly at the beginning during the low density phase, but due

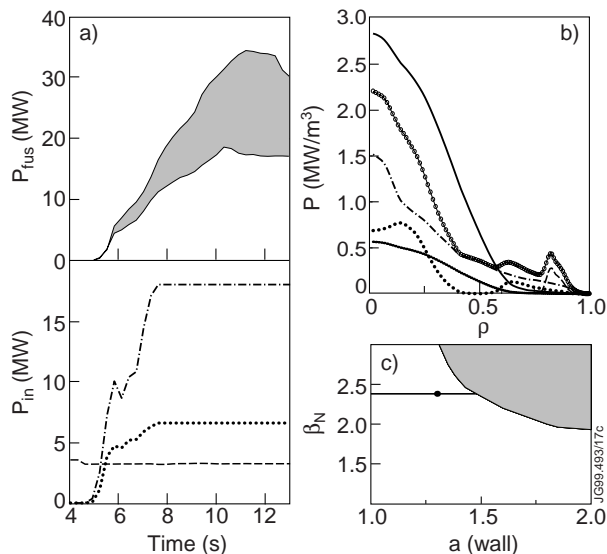


Figure 17. (a) Time evolution of the fusion power calculated by the two different transport models and the input powers (NB, chain curve; RF, dotted curve; LH, dashed curve). (b) Radial profiles of the input heating powers (NB, chain curve; RF, dotted curve; LH, dashed curve; NB+RF+LH, solid curve with circles) and produced fusion (solid curve) and alpha heating powers (densely dotted curve) with the transport model of the smaller particle diffusion coefficient (set 1) at $t = 13.0$ s. (c) MHD stability analysis of the scenario with the largest fusion power at $t = 13.0$ s. The shaded area is unstable with $n = 1$ kink instability as the limiting factor.

to the continuous density rise with beam fuelling it starts to decrease after $t = 7.0$ s. The electron temperature remains fairly constant after $t = 6.0$ s whereas the density rises until $t = 10.0$ s. The quasi-stationary regimes for electron and ion temperatures and densities, the pressure and the location of the ITB are reached at $t = 10$ s. The current diffusion time is around 40–50 s, but before $t = 20$ s it does not affect significantly the profiles or the footpoint of the ITB. The expansion of the ITB occurs mostly between $t = 5.3$ s and $t = 6.0$ s. One reason for the expansion of the ITB with time is the broadening of the low magnetic shear region as shown in Fig. 16(d), which can be explained by the applied $P_{LH} = 3.5$ MW LHCD and the continuous current rampup until $t = 9.5$ s. The magnetic shear is negative inside about 50–70% of the plasma radius. q_{95} is between 3 and 4 and settles during the steady state phase down to 3.1. Worth noticing is also the large contribution ($\approx 50\%$) from the bootstrap current which is produced in the large pressure gradient

region, i.e. in the same region where the footpoint of the ITB is located, thus giving rise to larger current and smaller magnetic shear in that region.

The time evolution of the fusion power is shown in Fig. 17(a) (upper half). The upper curve is obtained with set 1 of the multipliers w_1 and w_2 and the lower one with set 2. By varying w_1 and w_2 in the ranges $w_1 = [0.8, 1.6]$ and $w_2 = [0.3, 0.6]$ (between set 1 and set 2), the shaded area between the two curves for the estimated fusion power is obtained. As can be seen, fusion power in the range 20–30 MW is predicted for $I_p = 3.9$ MA, $B_t = 3.4$ T discharges. Flat-top conditions are obtained at $t \approx 10$ s, after about 5 s from the start of the main heating phase with input heating powers of $P_{NB} = 18$ MW, $P_{RF} = 6.5$ MW (composed of two thirds on-axis and one third off-axis deposition) and $P_{LH} = 3.5$ MW as illustrated in Fig. 17(a) (bottom).

The same two simulations (set 1 and set 2) as shown in Figs 15 and 17 were also performed without LHCD. In each run, the ITB was formed slightly later and its width stayed about 10 cm narrower until $t = 7.0$ s than in the simulation with LHCD. After $t = 7.0$ s the ITB started to shrink and finally, at $t \approx 8$ s, the width of the ITB settled down to $\rho \approx 0.4$. The fusion power was only about 50–60% of the fusion power with LHCD and the average ion temperature about 80%.

The predicted fusion power in fact exceeds clearly the total external input power over the whole plasma core region as shown in Fig. 17(b). The case with the larger fusion power (set 1) is stable against MHD instabilities with a beta value $\beta_N \approx 2.4$ as is seen as a point on the $\beta_N \approx 2.4$ curve in Fig. 17(c) and has a limit of $\beta_N \approx 3$, including wall stabilization with a wall at $r/a = 1.3$ compatible with previous JET results. The most limiting instability is the pressure driven global $n = 1$ kink instability which is a typical limiting factor for the high performance OS discharges in the DB mode on JET [28]. However, this MHD stability analysis does not concern tearing modes nor $q = 2$ ‘snakes’, which limit the high performance of JET OS plasmas.

Recent experiments on JET have shown that in the DB mode density does not increase with time in the way predicted by our transport model. In experiments density typically saturates at a level of $(4-5) \times 10^{19} \text{ m}^{-3}$, whereas the ion temperature continues to rise to 40 keV. However, ion temperatures saturated at the level of 15–20 keV with continuous density rise would be more desirable for reaching the highest fusion performance. The best OS

discharges on JET maintain quasi-steady-state conditions for up to three energy confinement times with neutron yields up to an equivalent of $Q_{DT} \approx 0.4$ at typical $\beta_N \approx 2$ [29]. The effect of the experimentally observed density saturation was not taken into account in our modelling calculations and, as a result, we may overestimate the fusion performance. With L mode plasma edge experiments, density is not saturated, but their problem is the disruptions caused by the pressure driven kink modes [5].

6. Summary and conclusions

LHCD control with transport calculations has been investigated with the JETTO transport code. JETTO has been upgraded by implementing the FRTC code that calculates, coupled with JETTO, LH power deposition and current density profiles. The heat transport model has been further tested in L mode and ELMy H mode with an ITB, and various particle transport models have been used in JETTO to model predictive high performance discharges in the OS DB operation mode. The JETTO transport model has been able to reproduce the formation and evolution of the ITBs in fair agreement, mostly within the experimental error bars, with experiments.

The LH power deposition profiles calculated by JETTO/FRTC are in good agreement with the profiles calculated by BRTC. Evolution of the q profile does not seem to depend on whether the LH power deposition and current density profiles are taken from FRTC or BRTC.

Improved ITB formation with off-axis LHCD calculated by JETTO/FRTC was found in transport calculations. LHCD provided wider ITBs and stiffened their location by reducing the magnetic shear in the OS regime. Current density profiles were hollow, and wider regions with reduced transport due to negative magnetic shear, as well as steady state conditions with more robust ITBs, could be sustained for a longer time. Without LHCD, q profiles were monotonic, whereas application of 3.5 MW LH power provided inverted q profiles across 50–70% of the plasma radius.

Four different current rampup schemes were analysed with JETTO. The total plasma current or the current rampup speed were varied keeping the other plasma parameters fixed. In the core region the current density profiles were not affected, but at larger radii they were strongly modified. ITBs were wider with larger currents and faster current rampup

speeds. In conclusion, shrinking of the ITBs is caused by higher edge shear, i.e. higher q_a (smaller I_p). Consequently, the best fusion performance for OS plasmas is expected to be obtained with the highest current and the fastest stable current rampup speed.

The transport modelling results for high performance JET plasma in the OS regime in DB mode at $I_p = 3.9$ MA, $B_t = 3.4$ T predicted a fusion power in the range of 20–30 MW with $Q \approx 0.7$ –1. Application of 3.5 MW LHCD was crucial in order to achieve the high performance because without LHCD the fusion power was only about 50–60% of the fusion power with LHCD and the ITB shrank from $\rho \approx 0.7$ to $\rho \approx 0.4$ when LHCD was not applied. Considerable uncertainties still exist, in particular, in the JET particle transport model. The peak performance was analysed to be stable against the kink and ballooning instabilities. However, even if the usually dominating $n = 1$ kink mode was stabilized, the MHD stability analysis did not include neoclassical tearing modes nor $q = 2$ snakes which can affect considerably the transport and lead to a soft rollover and thus limit the performance and the duration of the high performance phase of the OS discharge.

One of the key elements during the high performance phase is the increase and evolution of the density [30]. Steady state conditions were achieved only 5 s after the beginning of the main heating and fuelling phase at $t \approx 10$ s. The limiting factor was the slow fuelling rate from NBI. Higher fuelling rates by additional gas puffing or pellet injection than available from NBI alone would be necessary to raise the core density and the global performance faster [31]. However, until now no ITB with additional gas puffing or pellet injection has been formed or sustained on JET and thus they were not included in the modelling calculations for improving the performance. The recently installed high field side pellet launcher on JET can provide a route to increasing density with pellet fuelling without losing the ITB.

In addition to the fuelling problem, the high performance DT OS discharges on the JET tokamak during DTE1 campaign were limited to less than 5 s duration due to technical restrictions on the high power heating systems and the neutron budget. However, in the light of our modelling results there is a reason to suppose that the high current DT OS pulses could be extended to truly steady state operation with no destruction of the ITB and no significant loss of performance. The key element is the efficient current profile control by LHCD during the high performance phase.

Acknowledgements

The authors are grateful to G. Huysmans for providing them with the MHD stability calculations. The authors also thank A. Piliya and A. Saveliev for implementing the FRTC ray tracing code into JETTO. The NB power deposition profile calculations with PENCIL by A. Bickley are also highly appreciated. Special thanks are also due to D. Heading and G. Corrigan for technical assistance.

References

- [1] JET Team (presented by F.X. Söldner), *Plasma Phys. Control. Fusion* **39** (1997) B353.
- [2] Levinton, F.M., et al., *Phys. Rev. Lett.* **75** (1995) 4417.
- [3] Strait, E.J., et al., *Phys. Rev. Lett.* **75** (1995) 4421.
- [4] Gormezano, C., JET Team, *Phys. Rev. Lett.* **75** (1995) 487.
- [5] Söldner, F.X., et al., *Nucl. Fusion* **39** (1999) 407.
- [6] Murakami, M., et al., in *Controlled Fusion and Plasma Physics* (Proc. 26th Eur. Conf. Maastricht, 1999), Vol. 23J, European Physical Society, Geneva (1999) 1213.
- [7] Voitsekhoitch, I., et al., *ibid.*, p. 957.
- [8] Genacchi, G., Taroni, A., JETTO: A Free Boundary Plasma Transport Code (Basic Version), Rep. ENEA RT/TIB 1988(5), ENEA (1988).
- [9] Esterkin, A.R., Piliya, A.D., *Nucl. Fusion* **36** (1996) 1501.
- [10] Baranov, Yu.F., et al., *Nucl. Fusion* **36** (1996) 1031.
- [11] Erba, M., et al., *Plasma Phys. Control. Fusion* **39** (1997) 261.
- [12] Erba, M., et al., Validation of a New Mixed Bohm/gyro-Bohm Transport Model on Discharges of the ITER Data-Base, Rep. JET-R(96)07, JET Joint Undertaking, Abingdon (1996).
- [13] Parail, V.V., et al., *Nucl. Fusion* **39** (1999) 429.
- [14] Baranov, Yu.F., et al., *Nucl. Fusion* **39** (1999) 1463.
- [15] Parail, V.V., et al., in *Controlled Fusion and Plasma Physics* (Proc. 26th Eur. Conf. Maastricht, 1999), Vol. 23J, European Physical Society, Geneva (1999) 181.
- [16] Smithe, D.N., et al., in *Radiofrequency Power in Plasmas* (Proc. 8th Top. Conf. Irvine, 1989), AIP, New York (1989) 338.
- [17] Cottrell, G.A., et al., *Nucl. Fusion* **39** (1999) 389.
- [18] Mantsinen, M.J., et al., *Plasma Phys. Control. Fusion* **41** (1999) 843.
- [19] Ekedahl, A., et al., *Nucl. Fusion* **38** (1998) 1397.
- [20] Hugon, M., et al., *Nucl. Fusion* **32** (1992) 33.
- [21] Moreau, D., et al., in *Plasma Physics and Controlled Nuclear Fusion Research 1992* (Proc. 14th Int. Conf. Würzburg, 1992), Vol. 1, IAEA, Vienna (1993) 921.
- [22] Gormezano, C., et al., in *Applications of Radiofrequency Power to Plasmas* (Proc. 12th Top. Conf. Savannah, 1997), AIP, New York (1997) 3.
- [23] Karney, C.F.F., Fisch, N.J., *Phys. Fluids* **22** (1979) 1819.
- [24] Heikkinen, J.A., et al., *Plasma Phys. Control. Fusion* **41** (1999) 1231.
- [25] Keilhacker, M., et al., *Nucl. Fusion* **39** (1999) 209.
- [26] Litaudon, X., *Plasma Phys. Control. Fusion* **40** (1998) A251.
- [27] Horton, L.D., et al., *Nucl. Fusion* **39** (1999) 993.
- [28] Huysmans, G.T.A., et al., in *Controlled Fusion and Plasma Physics* (Proc. 24th Eur. Conf. Berchtesgaden, 1997), Vol. 21A, European Physical Society, Geneva (1997) 21.
- [29] Zastrow, K.-D., et al., in *Controlled Fusion and Plasma Physics* (Proc. 26th Eur. Conf. Maastricht, 1999), Vol. 23J, European Physical Society, Geneva (1999) 217.
- [30] Sips, A.C.C., et al., *Plasma Phys. Control. Fusion* **40** (1998) 1171.
- [31] Söldner, F.X., et al., in *Controlled Fusion and Plasma Physics* (Proc. 26th Eur. Conf. Maastricht, 1999), Vol. 23J, European Physical Society, Geneva (1999) 185.

(Manuscript received 11 October 1999

Final manuscript accepted 14 June 2000)

E-mail address of T.J.J. Tala: tuomas.tala@vtt.fi

Subject classification: H1, Tm; F1, Ti; F2, Ti; B0, Ti